RESEARCH ARTICLE

High-Accuracy Visible Light Positioning Algorithm Using Single LED Lamp With a Beacon

JIANWEI CHEN[ID]**, YI ZHANG**[ID]**, SHENG HE**[ID]**, AND XIANG LU**[ID]
School of Physical Science and Engineering Technology, Guangxi University, Nanning 530000, China
Corresponding author: Xiang Lu (xianglu@gxu.edu.cn)

ABSTRACT This paper presents a novel indoor visible light positioning algorithm utilizing single light emitting diode (LED) light. In the proposed system, a commercial circular LED light with a beacon and a smartphone served as the transmitter and receiver, respectively. By using the pixel information of the beacon for optical center and position correction, combined with the proportional relationship between the image and the world coordinate scale, precise world coordinates of the receiver can be accurately determined. This algorithm offers a simplified approach without the need for complex mathematical derivations, effectively reducing computational complexity without the need to restrict the orientation of the receiver in the horizontal plane. To validate the effectiveness of the proposed algorithm, an experimental setup has been constructed and tested. Experimental results demonstrate an average positioning error of 1.17 cm at a height of 2 m and a remarkably low average positioning error of 1.00 cm at a height of 1.5 m. The average positioning time of the system is 16.38ms.

I. INTRODUCTION

With the limitations of indoor GPS satellite positioning becoming more pronounced, visible light positioning (VLP) technology has emerged as an effective solution for indoor positioning [1]. Traditional wireless positioning methods commonly employed indoors include Wi-Fi, Zigbee, infrared, Bluetooth, ultrasonic, and ultra-wide- band (UWB) [2], [3], [4], [5], [6], [7]. However, these methods are plagued by challenges, such as limited accuracy and high cost. In contrast, visible light indoor positioning offers several compelling advantages, including cost-effectiveness, environmental sustainability, and superior accuracy [8].

VLP can be classified into two categories based on the type of receiver: photodetector (PD)-based positioning techniques and image sensor (IS)-based techniques. Among these categories, IS-based VLP technology has attracted significant

The associate editor coordinating the review of this manuscript and approving it for publication was Yong Yang[ID].

attention from researchers owing to its superior positioning accuracy compared with PD-based approaches, without the need for additional equipment. In [9], the authors propose a VLP system incorporating rectangular LEDs with inertial measurement units (IMU), demonstrating positioning errors averaging less than 4.5 cm. However, positioning time is also a crucial metric for evaluating VLP systems. In [10], the authors enhance system robustness using a particle filter method, achieving an accuracy of 2.95 cm with an average computation time of 21 ms. Additionally, some studies employing specific cameras as receivers have been reported [11], [12]. However, traditional IS-based VLP systems typically require the detection of at least three light emitting diode (LED) lights to establish the necessary positioning equations. Insufficient LED lights within the field of view can lead to positioning failure. To address the aforementioned challenges, many VLP systems using a single LED have been proposed [13], [14], [15], [16], [17], [18], [19], [20]. In [13], a single LED positioning algorithm based on circular projection is proposed, achieving

a positioning accuracy of 17.52 cm by employing ellipse fitting to derive projection information and integrating it with directional information provided by markers. However, the algorithm's high complexity resulting from circular projection introduces the system processing speed. In [14], a method utilizing square LEDs for calibrating the angle of a geomagnetic sensor is presented, maintaining positioning accuracy within 10 cm when the horizontal distance between the camera and the center of the LED is less than 120 cm, with an average positioning delay of approximately 39.64 ms. However, this method requires specific LED shapes and restricts the orientation of the luminaires. In [15], the authors classify LEDs using machine learning, achieving an accuracy of 7.39 cm with a computation time of 43.05 ms. Nevertheless, employing this LED classification approach necessitates capturing numerous images for offline training, implying increased human resource costs for system deployment. References [17], [18], [19], [21], and [22] utilize the built-in inertial measurement unit of smartphones, including accelerometers and gyroscopes, to provide additional positioning information, enabling centimeter-level positioning accuracy. However, IMUs are prone to cumulative errors that render them less reliable over time, leading to some positioning inaccuracies. Although these existing indoor positioning systems based on a single LED light can achieve sub-meter or even centimeter-level positioning accuracy, addressing the limitation of traditional VLP systems that require the detection of three LED lights, most of these systems still necessitate additional units or expensive dedicated receivers to achieve positioning, thereby significantly increasing system complexity and costs.

To address the aforementioned limitations, this paper introduces a novel indoor positioning algorithm based on a single LED with a beacon. This algorithm leverages the pixel information of the beacon to perform precise optical center and position calibration on images captured by a smartphone. By utilizing the scale relationship between the image and world coordinates, accurate world coordinates of the receiver can be determined. Notably, the system requires no additional equipment and does not need to constrain the orientation of the receiver on the horizontal plane. Moreover, the algorithm demonstrates excellent portability as it only necessitates the capture of three reference images for positioning in various indoor environments. To validate the algorithm's effectiveness, a comprehensive experimental setup was meticulously configured. The experimental results convincingly demonstrate that the proposed algorithm achieves remarkable positioning accuracy, with an average error of 1.17 cm at a height of 2 m, and an impressive error of only 1.00 cm at a height of 1.5 m.

II. SINGLE LED SYSTEM
A. SYSTEM ARCHITECTURE
The system architecture proposed in this study is illustrated in Fig. 1. The system comprises a transmitter and a receiver.
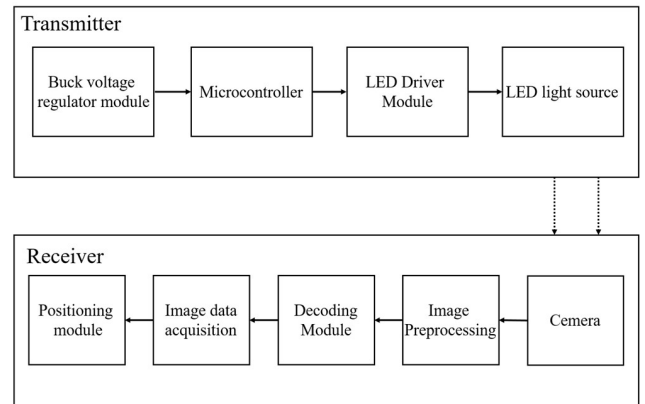

FIGURE 1. The proposed system architecture.

The transmitter consists of a buck voltage regulator module, a microcontroller, an LED driver module, and LED lights connected in sequence. The receiver is a commercially available smartphone equipped with a camera and integrated with modules for image preprocessing, decoding, image data acquisition, and positioning.

The light source in the VLP system consists of a LED downlight that repetitively broadcasts specific information, along with a non-flickering LED bead attached to the lamp's edge. To ensure efficient transmission of the specific information, the data is encoded using interleaved two of five (ITF) code [23]. Subsequently, the encoded data is modulated onto the LED driver module using widely applied and practical on-off keying (OOK) modulation [24]. In this modulation scheme, a "1" is represented by the LED being turned on, while a "0" is represented by the LED being turned off. This approach enables the repetitive broadcasting of the specific information through the LED lamp. After configuring the ISO and other parameters of the image sensor, bright and dark stripes are formed. Additionally, the modulation frequency of the LED has specific requirements. Typically, the modulation frequency must not fall below 200 Hz to ensure the human eye cannot perceive light flickering [25]. The upper limit frequency is usually determined by the resolution of the image sensor. If a frequency higher than the upper limit is used for driving, the captured image may suffer from the mixing of adjacent stripes, leading to decoding difficulties. Consequently, we set the driving frequency at 20 kHz, which surpasses the 200 Hz threshold and does not cause any discomfort to the human eye.

B. IMAGE PREPROCESSING
To decode the captured images, a series of preprocessing steps are applied to the raw images. Initially, the original images are converted to grayscale and subsequently binarized.

Following this, dilation operations are performed on the images. To guarantee the formation of closed regions, two successive dilations employ the same kernel. Subsequently,
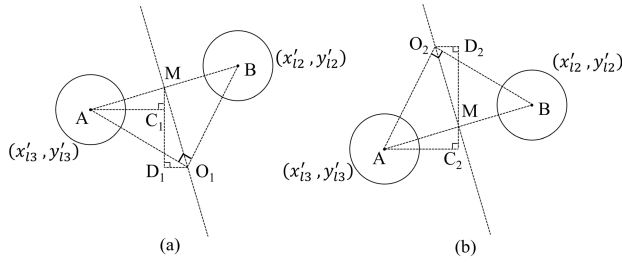
FIGURE 2. Geometric diagram of optical center: (a) O1; (b)O2.

FIGURE 3. The angle correction: (a) before correction; (b) after correction.

a mean filter is utilized to filter the resulting image, effectively removing noise. Finally, Hough circle detection is employed to identify the centroids and radii of the main LED lamp and beacon within the formed closed regions.

C. OPTICAL CENTER CALIBRATION

In the image coordinate system, the point where the optical axis of the camera intersects the imaging plane is generally considered as the center position. However, deviations from this ideal intersection point may arise due to potential imperfections in the camera manufacturing process. In positioning algorithms that heavily depend on this intersection point, even minor discrepancies in the pixel coordinates of this point can lead to substantial positioning errors.

This section presents a straightforward method for optical center calibration. Initially, two reference images, namely reference image 1 and reference image 2, are captured within the field of view. Subsequently, the camera is horizontally rotated 90 degrees around the optical center at one of the points, resulting in the capture of reference image 3. Specifically, in this study, reference image 2's corresponding point is rotated 90 degrees around the optical center to obtain reference image 3. The reference images are then subjected to the image preprocessing steps discussed in the previous section. This enables us to obtain the pixel coordinates of the main LED lamp $(x_{l1}{'}, y_{l1}{'})$ and beacon $(x_{b1}{'}, y_{b1}{'})$ for reference image 1, $(x_{l2}{'}, y_{l2}{'})$ and $(x_{b2}{'}, y_{b2}{'})$ for reference image 2, $(x_{l3}{'}, y_{l3}{'})$ and $(x_{b3}{'}, y_{b3}{'})$ for reference image 3. As reference image 3 is obtained through horizontal rotation of reference image 2 around the optical center, the actual optical center lies on the perpendicular bisector of the line segment connecting the centers of their main LED lamps. The geometric representation of optical center O_1 is depicted in Fig. 2(a), where A represents the center of reference image 3's main LED lamp, and B represents the center of reference image 2's main LED lamp. Based on the properties of the isosceles right triangle ABO_1, the following derivation is straightforward:

$$\Delta AC_1M \cong \Delta MD_1O_1 \tag{1}$$

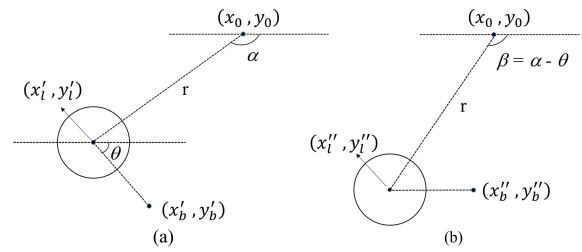According to (1), we can obtain the optical center O_1 (x_1, y_1):

$$x_1 = \frac{x_{l2}' + x_{l3}'}{2} + \left(y_{l3}' - \frac{y_{l2}' + y_{l3}'}{2}\right) \tag{2}$$

$$y_1 = \frac{y_{l2}' + y_{l3}'}{2} + \left(\frac{x_{l2}' + x_{l3}'}{2} - x_{l3}'\right) \tag{3}$$

Similarly, as shown in Fig. 2(b), we have the geometric representation of optical center O_2, where A represents the center of reference image 3's main LED lamp and B represents center of reference image 2's main LED lamp. In the same manner, we can derive:

$$\Delta AC_2M \cong \Delta MD_2O_2 \tag{4}$$

According to (4), we can obtain the optical center O_2 (x_2, y_2):

$$x_2 = \frac{x_{l2}' + x_{l3}'}{2} - \left(y_{l3}' - \frac{y_{l2}' + y_{l3}'}{2}\right) \tag{5}$$

$$y_2 = \frac{y_{l2}' + y_{l3}'}{2} - \left(\frac{x_{l2}' + x_{l3}'}{2} - x_{l3}'\right) \tag{6}$$

After obtaining optical centers O_1 and O_2, it is necessary to determine the true optical center. Since the deviation between the intersection point of the camera's optical axis and the imaging plane caused by camera manufacturing processes is usually small, we can compare the distances between O_1 and the center point of the imaging plane (L_1) and between O_2 and the center point of the imaging plane (L_2). We select the point with the shorter distance as the corrected true optical center.

D. POSITIONING ALGORITHM

Traditional positioning algorithms are limited in that they can only locate a specific camera pose, which significantly restricts their applicability. Therefore, in this paper, we address this limitation by performing angle correction on the images captured at the measured point, enabling the receiver to handle the angular deviations around the Z-axis (i.e. azimuth angle) and avoid significant positioning errors. Firstly, we define the obtained true optical center from the previous section as O (x_0, y_0). Fig. 3(a) illustrates the original image of the measured point before correction. We need to rotate the main LED lamp and the beacon around the optical center until the y-pixel coordinate of the main LED lamp is equal to the y-pixel coordinate of the beacon. Based on

Fig. 3(a), we can derive the following equation:

$$\alpha = \arctan \frac{y_l' - y_0}{x_l' - x_0} \tag{7}$$

where α is the angle between the line segment connecting the main LED lamp's center and the true optical center and the horizontal direction, (x_0, y_0) is the pixel coordinates of the true optical center O, and (x_l', y_l') is the pixel coordinates of the main LED lamp's center at the measured point.

Similarly, we have:

$$\theta = \arctan \frac{y_b' - y_l'}{x_b' - x_l'} \tag{8}$$

where θ is the angle between the line segment connecting the main LED lamp's center and the beacon and the horizontal direction, (x_b', y_b') is the pixel coordinates of the beacon.

Fig. 3(b) illustrates the state of the main LED lamp and the beacon after angle correction. Based on the positional relationship and coordinate information depicted in Fig. 3, we can determine the angle between the line segment connecting the center of the main LED lamp and the true optical center and the horizontal direction:

$$\beta = \alpha - \theta \tag{9}$$

After performing angle correction on the original image, we can easily obtain the pixel coordinates of the corrected main LED lamp's center:

$$x_l'' = x_0 + r \cos \beta \tag{10}$$
$$y_l'' = y_0 + r \sin \beta \tag{11}$$
$$r = \sqrt{(x_l' - x_0)^2 + (y_l' - y_0)^2} \tag{12}$$

where (x_l'', y_l'') is the pixel coordinates of the corrected main LED lamp's center, and r is the length of the line segment connecting the main LED lamp's center and the true optical center.

After obtaining the pixel coordinates of the corrected main LED lamp, the world coordinates of reference point 1 and reference point 2 corresponding to reference images 1 and 2, respectively, can be used to determine the physical distances in the x and y directions in the world coordinate system. The pixel coordinates of the main LED lamp in reference images 1 and 2 can be used to calculate the pixel distances in the x and y directions in the pixel coordinate system. For the x-axis, we can obtain the physical length corresponding to one pixel (k_1) and the offset (B_1):

$$k_1 = \frac{x_{l1} - x_{l2}}{x_{l1}' - x_{l2}'} \tag{13}$$
$$B_1 = x_{l1} - k_1 x_{l1}' \tag{14}$$

Similarly, in the y-axis direction, we can calculate the physical length corresponding to one pixel (k_2) and the offset (B_2):

$$k_2 = \frac{y_{l1} - y_{l2}}{y_{l1}' - y_{l2}'} \tag{15}$$
$$B_2 = y_{l1} - k_2 y_{l1}' \tag{16}$$

TABLE 1. Device parameters details.

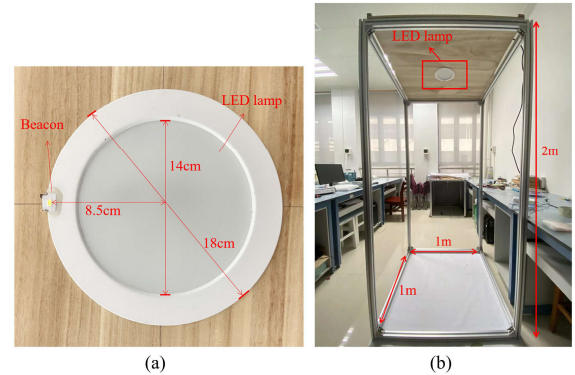| Component/Parameter	Model/Value
LED model	XHTDC 620(6500K)
Diameter/cm	14
Power/W	20
Camera model	Vivo Y3 rear camera
Focal length/mm	4
Image pixel resolution	4160×3120
Camera exposure time/ms	0.08

FIGURE 4. Schematic diagram of experimental setup: (a) LED downlight; (b) Experimental setup.

where (x_{l1}, y_{l1}) and (x_{l2}, y_{l2}) are the world coordinates of reference point 1 and reference point 2, respectively, and (x_{l1}', y_{l1}') and (x_{l2}', y_{l2}') are the pixel coordinates of the main LED lamp in reference images 1 and 2, respectively.

By establishing a linear equation regarding the physical length k and offset B, the world coordinates of the measured point can be obtained:

$$x = k_1 x_l'' + B_1 \tag{17}$$
$$y = k_2 y_l'' + B_2 \tag{18}$$

where (x, y) is the world coordinates of the measured point, and (x_l'', y_l'') is the pixel coordinates of the corrected main LED lamp.

III. EXPERIMENTAL SETUP AND RESULTS

To validate the effectiveness of the proposed optical center calibration method and the positioning algorithm, we conducted experiments to evaluate its performance. We used a common commercial LED downlight with a constant light bead added to the edge, as illustrated in Fig. 4(a), set an experimental setup with dimensions of 1 m x 1 m x 2 m, and installed the LED lamp at the top, with the world coordinates at (50, 50, 200), as depicted in Fig. 4(b). We conducted tests on planes at heights of 2 m and 1.5 m to ensure the algorithm's effectiveness. The receiver was a regular smartphone with a shutter speed set to 1/12000 s. The LED driving frequency was set to 20 kHz, which does not cause flickering to the human eye. The relevant parameters are shown in Table 1.

TABLE 2. Comparison of related work.

Related Work	Average Error/cm
Reference[13]	17.52
Reference[15]	7.39
Reference[16]	2.26
Reference[20]	7.2
Our work	1.17

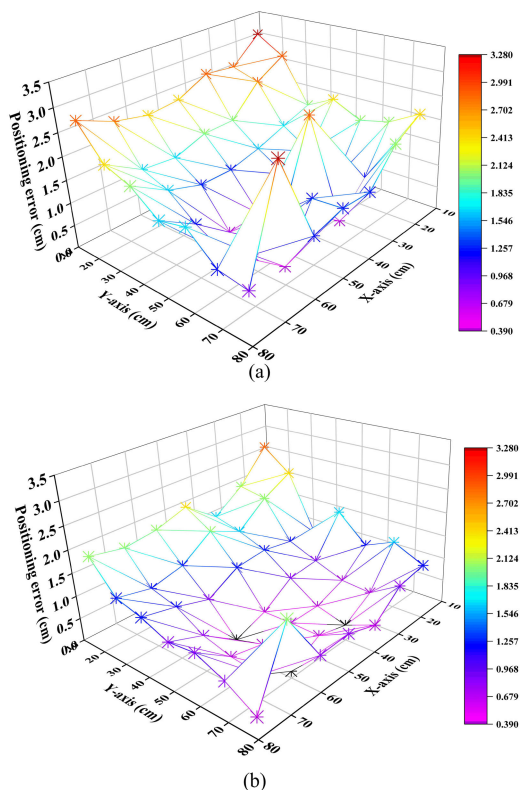**FIGURE 5.** Positioning error distribution map at a height of 2m: (a) Before calibration; (b) After calibration.

FIGURE 6. Positioning error distribution map at a height of 1.5m: (a) Before calibration; (b) After calibration.

To mitigate the influence of random errors, we conducted tests at 49 points on each height plane. For each test point, we captured 5 photos by changing the azimuth angle, and the final positioning result for each test point was represented by the average value. Fig. 5 and 6 show the distribution of average positioning errors before and after optical center calibration for the two heights. At a height of 2 m, the positioning errors before optical center calibration are overall greater than those after employing the optical center calibration method. After applying the optical center calibration method, the average positioning error within a 1 m x 1 m area reached 1.17 cm, with a minimum error of 0.05 cm and a maximum error of 2.95 cm for a single measurement. At a height of 1.5m, the difference in errors before and after optical center calibration becomes more pronounced. Following the application of the optical center calibration method, the average positioning error within a 1 m x 1 m area decreased to 1.00 cm, with a minimum error of 0.02 cm and a
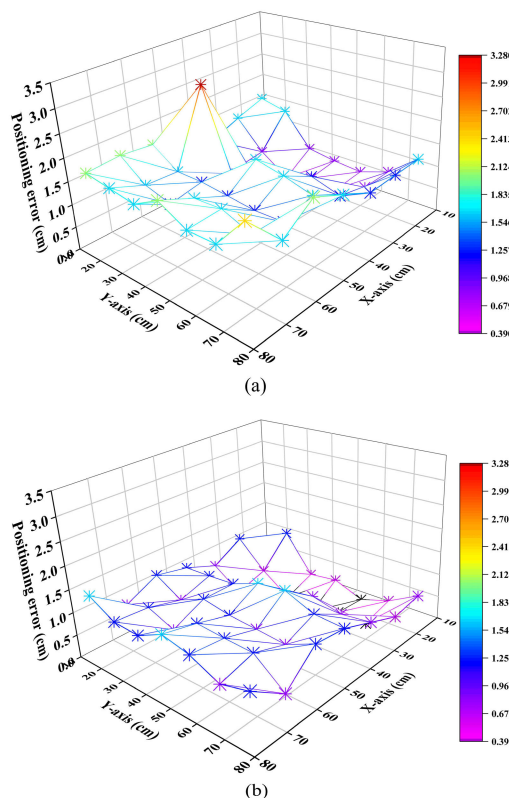
maximum error of 1.91 cm for a single measurement. It can be observed from the figures that the average positioning error is smaller at a height of 1.5 m, and the error distribution is more uniform compared to a height of 2 m. This is because when the camera is closer to the LED lamp, the captured image area is larger. This means that more pixels are occupied, resulting in more accurate identification of the centroid pixel coordinates. Fig. 7 and 8 provide an X-Y view of the five measurements before and after optical center calibration for two heights compared to the true coordinates. It is observable that the overall distribution after employing the optical center calibration method is superior to that before for both heights.

Fig. 9 and 10 respectively present the cumulative density function (CDF) of the positioning errors before and after applying the optical center calibration method for the two different heights. From the graph, it can be observed that at a height of 2 m, after employing the optical center calibration method, 90% of the positioning errors are within 2.21 cm. At a height of 1.5 m, after employing the optical center calibration method, 90% of the positioning errors are within 1.51 cm. This demonstrates that our proposed positioning algorithm achieves satisfactory positioning accuracy. In order to more intuitively demonstrate the superiority of the algorithm, we have compared the algorithm proposed in this paper with some reports that similarly utilize a single LED and beacon, as shown in Table 2.
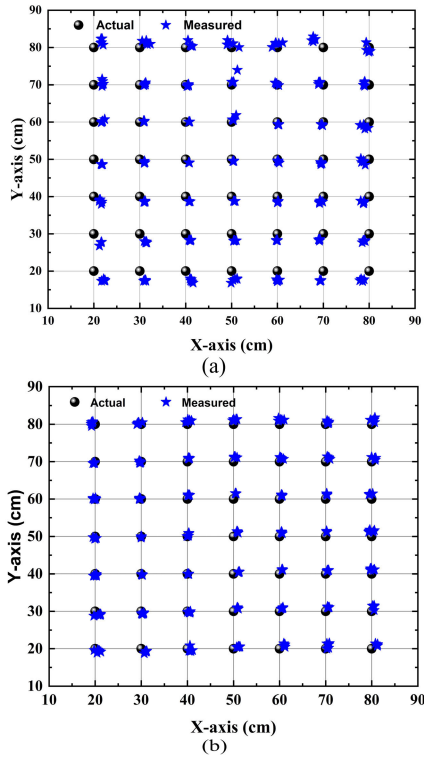
FIGURE 7. X-Y view of the five measurements with the real position at a height of 2m: (a) Before calibration; (b) After calibration.
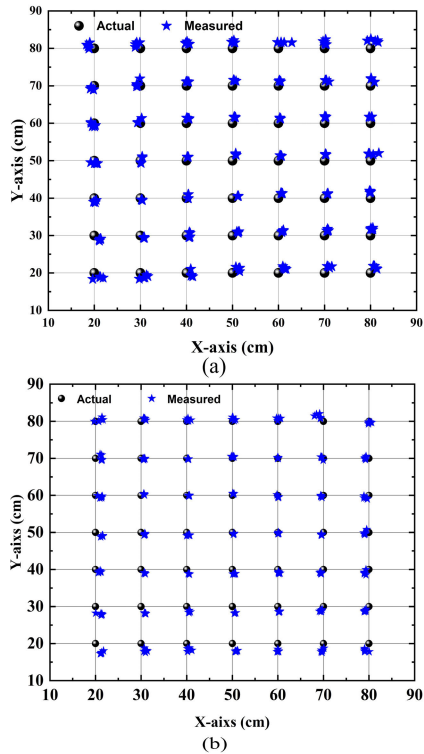

FIGURE 8. X-Y view of the five measurements with the real position at a height of 1.5m: (a) Before calibration; (b) After calibration.

FIGURE 9. The CDF diagram of 2m.

FIGURE 10. The CDF diagram of 1.5m.
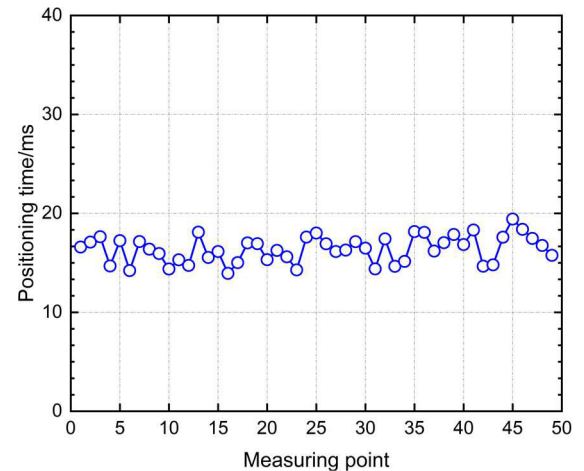
FIGURE 11. Average positioning time of the system.

Additionally, in practical positioning systems, key metrics for evaluating an algorithm include time complexity and space complexity. Among thes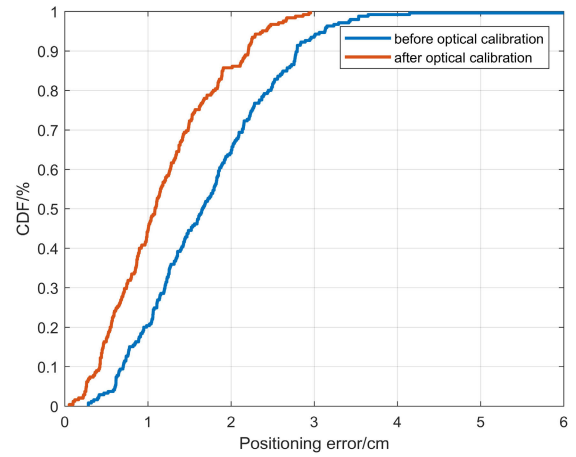e, 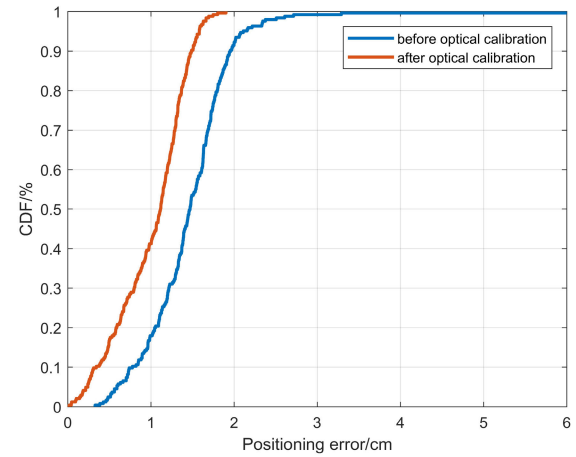time complexity can be determined by the positioning time, where algorithms with lower time complexity can effectively reduce the system's positioning time. We conducted tests on the positioning time of 49 selected points in the experiment, with each point being

measured 10 times; the average value of these measurements was taken as the positioning time for each point. The results, as shown in Fig. 11, indicate that the positioning time for all test points is below 20 ms, with a maximum single positioning time of 35.19 ms. The system's average positioning time is 16.38 ms, which is less than half of the positioning time reported in [14]. Space complexity is a measure of the amount of storage space temporarily occupied during system operation. As demonstrated in the algorithm process above, our proposed algorithm does not involve high storage-intensive operations such as matrix calculations. This demonstrates that the positioning algorithm we propose can effectively reduce algorithm complexity, thereby further decreasing the system's computational time.

IV. CONCLUSION
This paper presents a novel indoor visible light positioning algorithm utilizing a single LED. The algorithm leverages the pixel information of beacon to accurately calibrate the optical center and position of the captured smartphone images. By establishing the scale relationship between the image and world coordinate systems, the algorithm determines the precise world coordinates of the receiver. Our proposed algorithm exhibits notable advantages, including low complexity, high accuracy, and no need to restrict the horizontal orientation of the receiver. Experimental results validate its effectiveness, demonstrating an average positioning error of 1.178 cm at a height of 2 m, with a minimum error of 0.05 cm and a maximum error of 2.95 cm for a single measurement. Similarly, at a height of 1.5 m, the average positioning error reduces to 1.005 cm, with a minimum error of 0.02 cm and a maximum error of 1.91 cm for a single measurement. The average positioning time of the system is 16.38ms, indicating that the proposed algorithm can effectively reduce the algorithm complexity.

DECLARATION OF COMPETING INTEREST
The authors declare that they have no known competing financial interests or personal relationships that could have appeared to influence the work reported in this article.

CODE AVAILABILITY
Code will be made available on request.

ACKNOWLEDGMENT
(Jianwei Chen and Yi Zhang contributed equally to this work.)

REFERENCES
[1] Y. Zhuang, L. Hua, L. Qi, J. Yang, P. Cao, Y. Cao, Y. Wu, J. Thompson, and H. Haas, "A survey of positioning systems using visible LED lights," *IEEE Commun. Surveys Tuts.*, vol. 20, no. 3, pp. 1963–1988, 3rd Quart., 2018.

[2] Z. Li and Y. Zhang, "Constrained ESKF for UAV positioning in indoor corridor environment based on IMU and WiFi," *Sensors*, vol. 22, no. 1, p. 391, Jan. 2022.

[3] S.-H. Fang, C.-H. Wang, T.-Y. Huang, C.-H. Yang, and Y.-S. Chen, "An enhanced ZigBee indoor positioning system with an ensemble approach," *IEEE Commun. Lett.*, vol. 16, no. 4, pp. 564–567, Apr. 2012.

[4] E. Martín-Gorostiza, M. A. García-Garrido, D. Pizarro, D. Salido-Monzú, and P. Torres, "An indoor positioning approach based on fusion of cameras and infrared sensors," *Sensors*, vol. 19, no. 11, p. 2519, Jun. 2019.

[5] C. Zhou, J. Yuan, H. Liu, and J. Qiu, "Bluetooth indoor positioning based on RSSI and Kalman filter," *Wireless Pers. Commun.*, vol. 96, no. 3, pp. 4115–4130, Oct. 2017.

[6] M. C. Pérez-Rubio, Á. Hernández, D. Gualda-Gómez, S. Murano, J. Vicente-Ranera, F. Ciudad-Fernández, J. M. Villadangos, and R. Nieto, "Simulation tool and online demonstrator for CDMA-based ultrasonic indoor localization systems," *Sensors*, vol. 22, no. 3, p. 1038, Jan. 2022.

[7] P. Lou, Q. Zhao, X. Zhang, D. Li, and J. Hu, "Indoor positioning system with UWB based on a digital twin," *Sensors*, vol. 22, no. 16, p. 5936, Aug. 2022.

[8] A. B. M. M. Rahman, T. Li, and Y. Wang, "Recent advances in indoor localization via visible lights: A survey," *Sensors*, vol. 20, no. 5, p. 1382, Mar. 2020.

[9] S. Sun, G. Li, Y. Gao, and L. Wang, "Robust dynamic indoor visible light positioning method based on CMOS image sensor," *Photogrammetric Eng. Remote Sens.*, vol. 88, no. 5, pp. 333–342, May 2022.

[10] Y. Wu, W. Guan, X. Zhang, M. Huang, and J. Cao, "Visible light positioning system based on CMOS image sensor using particle filter tracking and detecting algorithm," *Opt. Commun.*, vol. 444, pp. 9–20, Aug. 2019.

[11] M. Wang, W. Ni, P. P. Shum, and C. Yang, "High-precision indoor visible light positioning with tilt receiver based on image sensors," in *Proc. Asia Commun. Photon. Conf. (ACP)*, Nov. 2022, pp. 546–550.

[12] G. Chen, W. Chen, Q. Yang, Z. Xu, L. Yang, J. Conradt, and A. Knoll, "A novel visible light positioning system with event-based neuromorphic vision sensor," *IEEE Sensors J.*, vol. 20, no. 17, pp. 10211–10219, Sep. 2020.

[13] R. Zhang, W.-D. Zhong, Q. Kemao, and S. Zhang, "A single LED positioning system based on circle projection," *IEEE Photon. J.*, vol. 9, no. 4, pp. 1–9, Aug. 2017.

[14] C. Yang, S. Wen, D. Yuan, J. Chen, J. Huang, and W. Guan, "CGA-VLP: High accuracy visible light positioning algorithm using single square LED with geomagnetic angle correction," *Photonics*, vol. 9, no. 9, p. 653, Sep. 2022.

[15] W. Guan, S. Wen, H. Zhang, and L. Liu, "A novel three-dimensional indoor localization algorithm based on visual visible light communication using single LED," in *Proc. IEEE Int. Conf. Autom., Electron. Electr. Eng. (AUTEEE)*, Nov. 2018, pp. 202–208.

[16] H. Li, H. Huang, Y. Xu, Z. Wei, S. Yuan, P. Lin, H. Wu, W. Lei, J. Fang, and Z. Chen, "A fast and high-accuracy real-time visible light positioning system based on single LED lamp with a beacon," *IEEE Photon. J.*, vol. 12, no. 6, pp. 1–12, Dec. 2020.

[17] W. Guan, L. Huang, S. Wen, Z. Yan, W. Liang, C. Yang, and Z. Liu, "Robot localization and navigation using visible light positioning and SLAM fusion," *J. Lightw. Technol.*, vol. 39, no. 22, pp. 7040–7051, Nov. 15, 2021.

[18] Y. Ji, C. Xiao, J. Gao, J. Ni, H. Cheng, P. Zhang, and G. Sun, "A single LED lamp positioning system based on CMOS camera and visible light communication," *Opt. Commun.*, vol. 443, pp. 48–54, Jul. 2019.

[19] J. Hao, J. Chen, and R. Wang, "Visible light positioning using a single LED luminaire," *IEEE Photon. J.*, vol. 11, no. 5, pp. 1–13, Oct. 2019.

[20] T. Wang, Z. Lin, H. Cheng, and C. Xiao, "Single LED visible light positioning system based on image sensor and calculated azimuth angle," *Appl. Opt.*, vol. 62, no. 4, pp. 886–893, Feb. 2023.

[21] Y. Hou, S. Xiao, M. Bi, Y. Xue, W. Pan, and W. Hu, "Single LED beacon-based 3-D indoor positioning using off-the-shelf devices," *IEEE Photon. J.*, vol. 8, no. 6, pp. 1–11, Dec. 2016.

[22] H. Cheng, C. Xiao, Y. Ji, J. Ni, and T. Wang, "A single LED visible light positioning system based on geometric features and CMOS camera," *IEEE Photon. Technol. Lett.*, vol. 32, no. 17, pp. 1097–1100, Sep. 15, 2020.

[23] J. Fang, Z. Yang, S. Long, Z. Wu, X. Zhao, F. Liang, Z. L. Jiang, and Z. Chen, "High-speed indoor navigation system based on visible light and mobile phone," *IEEE Photon. J.*, vol. 9, no. 2, pp. 1–11, Apr. 2017.

[24] F. Yang, J. Gao, and S. Liu, "Novel visible light communication approach based on hybrid OOK and ACO-OFDM," *IEEE Photon. Technol. Lett.*, vol. 28, no. 14, pp. 1585–1588, Jul. 1, 2016.

[25] C. Xie, W. Guan, Y. Wu, L. Fang, and Y. Cai, "The LED-ID detection and recognition method based on visible light positioning using proximity method," *IEEE Photon. J.*, vol. 10, no. 2, pp. 1–16, Apr. 2018.

SHENG HE was born in Guangxi, China, in 2001. He is currently pursuing the B.E. degree with the School of Physical Science and Engineering Technology, Guangxi University. His research interests include visible light communications and machine vision.

JIANWEI CHEN received the B.E. degree in electronic science and technology from Guangxi University, in 2020, where he is currently pursuing the M.S. degree with the School of Physical Science and Engineering Technology. His main research interests include visible light communications and positioning technology.

YI ZHANG was born in Jiangxi, China, in 2002. She is currently pursuing the B.E. degree with the School of Physical Science and Engineering Technology, Guangxi University, focusing on the research of visible light positioning and machine vision.

XIANG LU received the M.S. degree in power systems and automation from Guangxi University, in 2007, and the Ph.D. degree in power electronics and power transmission from the South China University of Technology, in 2015. His current research interests include visible light communications and visible light positioning systems.

• • •